J. Phys. B: At. Mol. Opt. Phys. **43** (2010) 205101 (9pp) doi:10.1088/0953-4075/43/20/205101

# Multiphoton population transfer between rovibrational states of HF: adiabatic rapid passage in a diatomic molecule

**Türker Topçu and Francis Robicheaux**

Department of Physics, Auburn University, AL 36849-5311, USA

E-mail: turker@physics.auburn.edu

Received 19 May 2010, in final form 20 August 2010
Published 27 September 2010
Online at stacks.iop.org/JPhysB/43/205101

**Abstract**

Efficient population transfer by adiabatically chirping through a multiphoton resonance in microwave driven and kicked Rydberg atoms has recently been reported both experimentally and theoretically. Here we report on our simulations in which we have exploited this mechanism to vibrationally excite a diatomic molecule up to $|\nu = 4, J\rangle$ from the ground state by chirping through a four-photon resonance condition. This is an efficient means of population transfer, which is an alternative to the ladder climbing scheme requiring chirping through a sequence of states in the correct order. We discuss and compare one-dimensional quantum and classical models where there is no rotational degree of freedom. This comparison suggests that for the lowest laser intensity we consider, the process is classically forbidden and the transition occurs through tunnelling. We show that for larger peak intensities, the transfer can be looked upon as a classical transition in phase space, similar to that observed in the atomic case. We extend our simulations to fully three-dimensional quantum calculations and investigate the effect of coupling between different rotational pathways. We finally discuss the effect of thermal averaging over the initial $J$-states using a temperature for which the first few rotational levels inside the $\nu = 0$ manifold are populated.

## 1. Introduction

Since femtosecond lasers became available in laboratories, creation of vibrationally excited molecules has led to important discoveries and applications. Apart from the fundamental physics aspect of these studies, steering chemical reactions emerged as a practical application since unlikely chemical reaction paths can become favoured by the excitation of certain rovibrational levels. Particularly, a large body of work has been devoted to the dissociation of small molecules using femtosecond lasers (see [1, 2]). Break-up of large molecules can also be controlled by the excitation of a particular rovibrational mode, which puts efforts devoted to the studies of selective vibrational excitation next to those towards dissociation [3–9]. The main methodology for exciting the vibrational states of molecules has been vibrational ladder climbing where the driving laser pulse is chirped through a series of single-photon resonances in order to transfer population into a desired final state. Short durations of femtosecond lasers have provided relatively large spectral bandwidths, which can potentially contain many frequencies desired to adapt to the vibrational evolution of the molecule.

A more recent use of vibrationally excited molecules is in quantum information science [10]. The possibility of implementing well-known classical algorithms using the effects of quantum interference relies on the availability of Bohr-like non-dispersing wave packets whose unitary evolution in time is necessary to perform computations. Such wave packets require near equally spaced energy levels in order to endure decoherence. One way this has been realized is by exposing very highly excited Rydberg atoms ($n \sim 300$) to a series of impulsive electric field kicks [11]. The fact that the difference in energy spacings between adjacent $n$-manifolds scales like $\sim 1/n^3$ means the energy change is $2/n$ times the energy spacing itself (given that energy scales $\sim 1/(2n^2)$). For $n = 300$, this translates into a change in energy that is $1/150$ of the energy of $n = 300$. This has been observed to be small enough for such highly excited Rydberg wave packets to survive for several Rydberg periods before

 

incoherence starts to become important. Short periods of vibrational oscillations and similarities to a harmonic oscillator make vibrationally excited molecules a potential candidate to be used in such studies. For example, a recent study has utilized vibrationally excited iodine molecules to perform an ultrafast discrete Fourier transform by tailoring a vibrational wave packet coupled to an electronic transition [12].

An efficient method of population transfer in a Li atom between its highly excited Rydberg states has been experimentally realized [13] by adiabatically chirping a microwave pulse through a ten-photon resonance condition. Starting from a state with the principle quantum number $n = 72$, they experimentally observed ~80% population transfer into the $n = 82$ manifold. The physical mechanism behind the process has been explained in terms of a quantum ten-photon transition (multiphoton adiabatic rapid passage) or equivalently by a classical transition in phase space [14] through classical and quantum simulations for microwave-driven [14] and kicked Rydberg atoms [15].

In this work, we utilize the same multiphoton adiabatic rapid passage mechanism [13, 14] to excite a ground-state diatomic molecule into a rovibrational excited state. Using HF as an example, we are able to simulate complete population transfer from the ground vibrational state $|\nu = 0, J\rangle$ into the $|\nu = 4, J\rangle$ manifold by chirping an IR laser through a four-photon resonance condition. The previously studied atomic cases and the molecular case studied in this work differ in the sense that the molecule starts in the ground vibrational state with the smallest possible classical action, while the Rydberg atom started in a highly excited state. It is reasonable to suspect that this can potentially lead to different mechanisms for the excitation process in both cases: the Rydberg atom has a very large number of states below and an infinite number of states above the initial state, whereas the molecule has no bound states below and a finite number of states above the initial state. The chirp range we needed to use is much smaller than that which would be needed when transferring population through ladder climbing, which requires chirping the laser through many single-photon transitions to reach the desired final state. The chirping of the laser removes the necessity to know the exact multiphoton resonance frequency, and the excitation process itself is not strongly dependent on the size of the chirp. The laser intensities we needed for exciting the population up to the $\nu = 4$ manifold from the ground state are of the order of $\sim 10^{13}$ W cm$^{-2}$, which is typical for multiphoton excitations in HF as reported previously in [16].

In section 2, we employ one-dimensional quantum and classical models to demonstrate that for a low-enough peak intensity for which the transition is classically forbidden, complete population transfer can be achieved quantum mechanically. For peak intensities high enough such that the transition is classically allowed, we observe the same classical separatrix crossing mechanism as discussed in [14, 15] leading to efficient population transfer. The effect of rotational coupling is taken into account in section 3 by extending the one-dimensional quantum model to full three dimensions. Particularly, we drive a four-photon resonance condition from $|\nu = 0, J = 1\rangle$ to $|\nu = 4, J\rangle$ in HF, and find that after the pulse is turned off, the entire population still resides in $J = 1$. The only rotational modes that get excited during the pulse are $J = 0$ and $J = 2$ that are adjacent to the initial $J = 0$ mode. This is very different than the behaviour observed in microwave-driven Rydberg atoms, where virtual transitions mix states up to very high-$\ell$ inside the final $n$ manifold. Finally, in section 4, we consider what would happen if we were to start from a thermal distribution of initial states over rotational modes instead of a vibrational eigenstate of HF.

We use atomic units throughout the paper unless specified otherwise.

## 2. One-dimensional models

### 2.1. Quantum calculations in one dimension

One-dimensional quantum calculations involved solving the time-dependent Schrödinger equation using a Morse potential to model the vibrational potential of HF. We use a lowest order implicit scheme for the time propagation of the Schrödinger equation and employ a radial mesh in space that extends out to 40 au using sufficient number of mesh points to obtain the molecular eigenenergies to less than a percent accuracy. In one dimension, the total molecular Hamiltonian is $H = -(1/2m)(\mathrm{d}^2/\mathrm{d}r^2) + V_M(r)$ with the Morse potential $V_M(r)$ given by

$$V_M(r) = D\left[\mathrm{e}^{-2\alpha(r-r_0)} - 2\mathrm{e}^{-\alpha(r-r_0)}\right]. \tag{1}$$

For HF, $D = 5.716$ eV is the dissociation energy, $r_0 = 1.75$ au is the equilibrium bond length, $\alpha = 1.22$ au and $m = 0.95$ amu is the reduced mass. Here the radial coordinate is restricted in the region $r \geqslant 0$, and the model resembles an s-wave model. Analytical solution for the time-independent Schrödinger equation exists for the one-dimensional case, and the energy $E_\nu$ is [17]

$$E_\nu = -D\left[1 - \frac{\alpha}{\sqrt{2mD}}\left(\nu + \frac{1}{2}\right)\right]^2, \tag{2}$$

and the number of bound states can be deduced from

$$\nu < \frac{\sqrt{2mD}}{\alpha} - 1/2. \tag{3}$$

For these sets of parameters, we have found that $\nu < 21.7$ meaning that 21 bound states exist in the vibrational spectrum of HF in the absence of any external field.

The interaction Hamiltonian describing the effect of the applied driving pulse is $-\mathcal{F}(t)\mu$, where we use a Gaussian carrier envelope as opposed to a flat-top envelope as in [15]:

$$\mathcal{F}(t) = F_{IR}\ \exp\left[-\left(\frac{t}{\Delta t}\right)^2\right]\cos[\omega t + \dot{\omega}t^2/2]. \tag{4}$$

The peak field strength $F_{IR}$ is proportional to the square-root of the laser intensity $\sim\sqrt{I}$. The central frequency $\omega$ of the transition is $\Delta E/N_{\mathrm{phot}}$, where $\Delta E$ is the energy difference between the ground state of HF and that of the targeted final state, and $N_{\mathrm{phot}}$ is the number of photons needed for the resonance condition. For the four-photon resonance condition we study below, $\omega = 0.0168$ au, which falls into the far

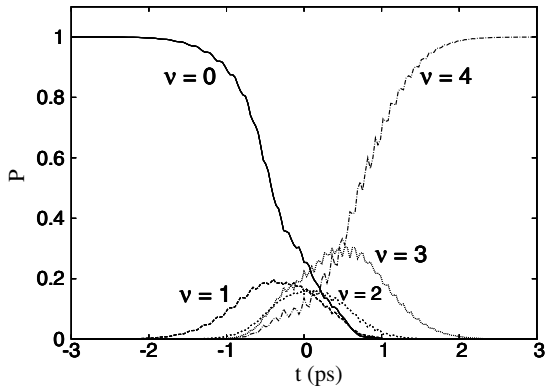


**Figure 1.** Time-dependent evolution of the probability $P$ to find the HF molecule in vibrational states with $\nu = 0$–4 for the four-photon resonance excitation from the ground state $\nu = 0$ to $\nu = 4$. The IR pulse has a peak intensity of $5 \times 10^{13}$ W cm$^{-2}$ and the carrier envelope centred at $t = 0$ ps has a width of 1.38 ps at FHWM.

infrared region of the electromagnetic spectrum. The chirp range for the laser field is $\dot{\omega} = 2s\ \omega/t_f$ with $s = 0.02 - 0.04$ resulting in a change in central frequency by 2–4%. Time steps taken during the propagation of the Schrödinger equation are chosen such that there are roughly 44 time points in each cycle of the infrared pulse. Time runs from $-t_f$ to $t_f$ which centres the peak of the carrier envelope at $t = 0$. We use the dipole function $\mu(r)$ for HF from [18] having the form $\mu(r) = A\ r \exp(-Br^4)$ with $A = 0.4541$ and $B = 0.0064$.

We evaluate the probability for finding the molecule in a given vibrational state by projecting the field-free eigenstates of HF onto the time-dependent wavefunction. These eigenstates are generated on the same radial mesh used for the time propagation by integrating the time-independent Schrödinger equation.

Figure 1 shows the time-dependent probabilities to find the HF molecule in vibrational manifolds $\nu = 0$–4 when it starts out in the $\nu = 0$ state and is driven up to $\nu = 4$ through the four-photon resonance condition. The driving intensity is $5 \times 10^{13}$ W cm$^{-2}$ and the carrier envelope is ∼1.38 ps at FWHM. The laser pulse is chirped from 2% of the four-photon resonance frequency below to 2% above the field-free resonance condition. The initial state $\nu = 0$ is completely depleted and the entire population ends up in $\nu = 4$. Although the intermediate states get populated during the transition at roughly 20−40% level, they all transition up to $\nu = 4$ after the pulse is turned off. For instance, at around 1 ps, the entire population is essentially in either $\nu = 3$ or $\nu = 4$ state, and $\nu = 3$ transitions into $\nu = 4$ at ∼2 ps. This is a direct consequence of the fact that the vibrational period changes little with energy and the anharmonicity of the vibrational energy levels is engrossed inside the chirp plus the bandwidth of the carrier envelope.

Instead of chirping through a multiphoton transition, if we wanted to transfer the population via a ladder climbing scheme like the one used in [4], we would have to induce a series of single-photon transitions: $0 \to 1$, $1 \to 2$, $2 \to 3$, and finally $1 \to 4$ starting from $\nu = 0$. The resonance frequency of the $0 \to 1$ transition would be needed to be decreased to keep up with the evolving vibrational distribution. In this scenario involving HF, we would have to chirp the $0 \to 1$ transition frequency down by more than ∼14% of its initial value to reach up to $\nu = 4$. Compared to the 2% chirp we needed as shown in figure 1, this is a relatively large chirp.

**Table 1.** Probabilities $P$ to find HF in vibrational states with $\nu = 0$ and $\nu = 4$ for various intensities $I$ (W cm$^{-2}$), chirp ranges and widths of the carrier envelope ($t_W$) in units of classical oscillation period $\tau_M$ of $\nu = 0$ for the one-dimensional quantum model discussed in the text.

| $I$ (W cm$^{-2}$) | Chirp | $t_W(\tau_M)$ | $P_{\nu=0}$ | $P_{\nu=4}$ |
|---|---|---|---|---|
| $5 \times 10^{13}$ | 2% | 168 | 0.00 | 1.00 |
| $1 \times 10^{13}$ | 2% | 168 | 0.93 | 0.07 |
| $1 \times 10^{13}$ | 2% | 336 | 0.87 | 0.13 |
| $1 \times 10^{13}$ | 2% | 672 | 0.75 | 0.25 |
| $5 \times 10^{12}$ | 2% | 672 | 0.99 | 0.01 |
| $5 \times 10^{12}$ | 2% | 1344 | 0.97 | 0.02 |
| $5 \times 10^{12}$ | 4% | 672 | 0.97 | 0.006 |

The peak intensity used in figure 1 is the lowest intensity at which we could get the system to transfer with 100% efficiency for the aforementioned pulse duration and chirp. Table 1 lists the final probabilities to find the system in $\nu = 0$ and $\nu$ states for various peak intensities $I$, chirp ranges and carrier envelope widths in units of classical vibrational periods $\tau_M$ corresponding to that of $\nu = 0$. Decreasing the peak intensity used in figure 1 by a factor of 5 down to $1 \times 10^{13}$ W cm$^{-2}$ results in only ∼4% transition probability into $\nu = 4$, and rest of the population stays in the initial $\nu = 0$ state. Note that this only corresponds to a decrease in the peak field strength by a factor of ∼2.2. At this point, doubling the carrier envelope width roughly doubles the final yield in $\nu = 4$, and the entire population still resides in states with $\nu = 0$ and 4. Further doubling the pulse width gives another factor of ∼2 in the final population inside the $\nu = 4$ state. Having quadrupled the carrier envelope width up to $672\tau_M$, decreasing the peak field intensity by a factor of 2 again reduced the final population inside $\nu = 4$ by roughly a factor of 25 down to ∼1%. Lengthening the pulse width to $1344\tau_M$ only gives a factor of 2 boost. In the case of the $672\tau_M$ pulse, doubling the chirp range from 2% to 4% also gives a factor of 2 drop in the final yield. In this very last case shown in table 1 where the chirp range is twice the size compared to a previous case with the same intensity and pulse width, ∼2% of the population goes up to $\nu = 3$ after the pulse intensity drops down by about 4 orders of magnitude towards the end of the pulse. This is a three-photon transition which is swept through during chirping over a larger frequency range close to the end of the pulse. In all the other cases in table 1, the entire population resides either in $\nu = 0$ or in $\nu = 4$.

For the transitioning depicted in figure 1, the magnitudes of the one-dimensional wavefunction in space at different points in time along the IR pulse envelope are plotted in fig 2. At half the peak intensity $2.5 \times 10^{13}$ W cm$^{-2}$ before the transition (figure 2(a)), the system is entirely in the initial $\nu = 0$ state. This roughly corresponds to $t = -1.12$ ps in figure 1 when ∼5% of the population is in the $\nu = 1$ state and the remaining ∼95% is in the initial state. At the

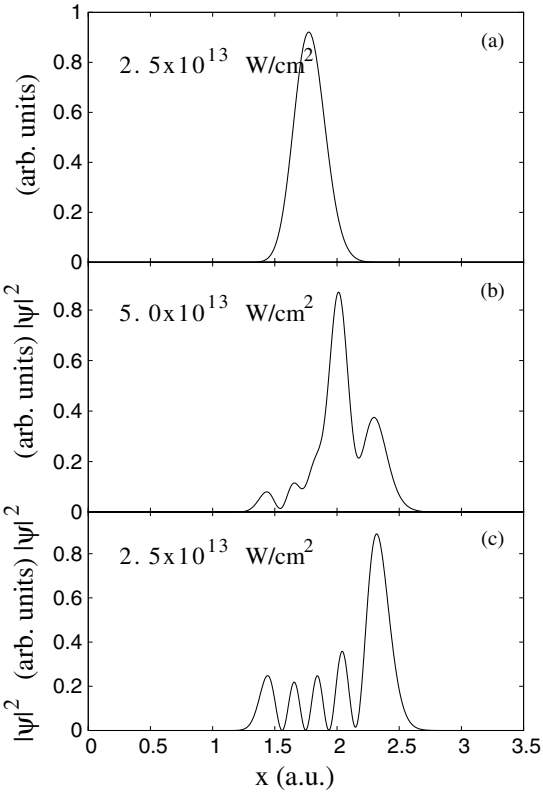


**Figure 2.** One-dimensional wavefunction amplitudes in space before (a), on (b) and after (c) the peak of the IR pulse for the same set of parameters used for figure 1. The spatial distribution in (a) is entirely that of the field-free $\nu = 0$ eigenstate of the HF molecule, and the one in (c) is almost entirely that of the $\nu = 4$ eigenstate.

peak of the pulse in figure 2(b), the system is clearly in a transitory state with nodes starting to form. At this point the wavefunction is a superposition of the states with $\nu = 0$–4 with mixing coefficients $\sqrt{P_\nu}$ seen in figure 1 at $t = 0$ ps. It can be speculated that since the wavefunction has nodes that do not go to zero, it is likely that it cannot be expressed as an eigenstate of some complicated Hamiltonian. In other words, it has a larger spread in momentum space than that would be covered by a superposition of the field-free eigenstates with real mixing coefficients. At half the peak intensity in figure 2(c), after the transition takes place, the molecule is mostly in the $\nu = 4$ state. This corresponds to about $t = 1.12$ ps in figure 1 when ∼15% of the population is in the $\nu = 3$ state with the remaining in $\nu = 4$.

### 2.2. *Classical calculations in one dimension*

The classical mechanism behind the population transfer using microwaves has been explained in [14] using a one-dimensional classical model. Since the transition is induced by chirping through a multiphoton resonance in the quantum picture, it is natural to expect that a well-defined sharp final state distribution would not result in the classical picture which lacks resonance concept. Surprisingly, authors observed that well-defined final state distributions also result from classical simulations. Tracing the classical trajectories in phase space,

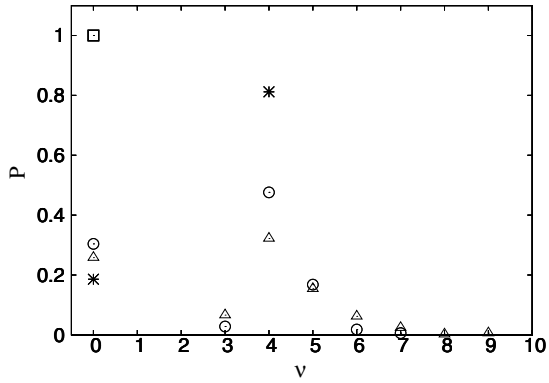


**Figure 3.** Final $\nu$-distributions from our one-dimensional classical model for the same pulse duration and chirp range used in the one-dimensional quantum calculation presented in figure 1 for various peak laser intensities. (□) $I = 5 \times 10^{13}$ W cm$^{-2}$, (∗) $I = 9 \times 10^{13}$ W cm$^{-2}$, (◯) $I = 13.5 \times 10^{13}$ W cm$^{-2}$, and (△) $I = 18 \times 10^{13}$ W cm$^{-2}$. In contrast with the one-dimensional quantum model, no transfer occurs for the peak intensity of $5 \times 10^{13}$ W cm$^{-2}$. We bin $\nu$ by taking its nearest integer value.

they investigated the classical mechanism responsible for the transition. Although there are no resonances in the classical picture, they found that microwave driving creates a stable island centred at roughly halfway between the initial and final states in classical action, which corresponds to $n$ for the Coulomb problem. The initial state just below the island and the final state above it form a separatrix at the right field strength. Driving the system a little harder destroys the separatrix and creates a chaotic sea, mixing the trajectories that were initially on the initial stable surface (i.e. initial state) into the chaotic sea. This narrow chaotic sea also borders the stable surface above the island of stability. During the falling edge of the driving pulse, the field strength becomes small enough so that the stable surfaces again form the separatrix and the initial final stable surfaces, which trap the trajectories that were mixed into the chaotic sea. By chirping the microwave frequency a small amount, most of the trajectories can be made to end up on the stable surface above the island of stability. In this section, we will demonstrate that the same separatrix crossing mechanism is also responsible for the vibrational population transfer observed in section 2.1.

In our classical simulations, we solve Hamilton's equations in one dimension using a fourth-order adaptive step-size Runga–Kutta method. We use the same Hamiltonian used in the one-dimensional quantum simulations except that we now use the $x$-coordinate instead of the radial coordinate with the same numerical parameters $x_0$ and $\alpha$. The interaction Hamiltonian is again $-\mathcal{F}(t)\mu$, where $\mu(x) = A\ x \exp(-Bx^4)$ with $A = 0.4541$ and $B = 0.0064$ as before, and the IR laser is polarized along the $x$-direction. The corresponding classical force from the Morse potential is

$$-\mathrm{d}V_M(x)/\mathrm{d}x = 2D\alpha\left[\mathrm{e}^{-2\alpha(x-x_0)} - 2\mathrm{e}^{-\alpha(x-x_0)}\right]. \qquad (5)$$

Figure 3 shows the final $\nu$-distribution of the transition probabilities for the four-photon resonance condition starting

from the ground state. An IR pulse with a carrier envelope of ∼1.38 ps at FHWM is used with a chirp range of 2% for various peak field intensities. We use 500 trajectories for each peak intensity and bin the final energy of the trajectories in $\nu$ after the IR pulse is turned off. We bin the population in $\nu$ according to equation 2 such that it is rounded off to the nearest integer. The squares in figure 3 are for $I = 5 \times 10^{13}$ W cm$^{-2}$, the stars are for $I = 9 \times 10^{13}$ W cm$^{-2}$, the circles are for $I = 13.5 \times 10^{13}$ W cm$^{-2}$, and the triangles are for $I = 18 \times 10^{13}$ W cm$^{-2}$. The square with $5 \times 10^{13}$ W cm$^{-2}$ peak intensity corresponds exactly to the one-dimensional quantum case presented in figure 1 and surprisingly shows that no vibrational transition has taken place. This is in stark contrast with the quantum result seen in figure 1 which displays entire population transitioning into the $\nu = 4$ state after the pulse is turned off. This suggests that the transition occurs as the wavefunction tunnels into the classically forbidden region and is a purely quantum effect at this field strength. We had to increase the peak intensity to $9 \times 10^{13}$ W cm$^{-2}$ (stars in figure 3), which is a factor of ∼1.3 increase in the peak field strength, to classically have ∼83% of the population to end up with $\nu = 4$ and ∼13% with $\nu = 0$. In this case, there is no spread in the final $\nu$-distribution, a behaviour also displayed classically using Rydberg atoms in our previous work [14]. Increasing the peak intensity to $13.5 \times 10^{13}$ W cm$^{-2}$ (circles) results in a final $\nu$ spread that covers from $\nu = 3$ to 7 with about half the population residing in $\nu = 4$. Further increase in the peak intensity to $18 \times 10^{13}$ W cm$^{-2}$ (triangles) widens the spread of final $\nu$ and results in roughly 10% dissociation (final $E > 0$). In this case, ∼34% of the population ends up in $\nu = 4$ and ∼19% stays in the initial state.

In order to probe the classical process taking place during the transition, we looked at one-dimensional surfaces of section plots in classical phase space as described in our previous work with microwave-driven and kicked Rydberg atoms [14, 15]. We use the action-angle variables $I$ and $\theta$ to picture the classical phase space. They are derived in [19] for the field-free Morse potential and are given by

$$I = 2\pi(\nu + 1/2)$$
$$\theta = \frac{1}{2\pi}\,\mathrm{sgn}(p)\cos^{-1}\left[\frac{z + E/D}{z\sqrt{1 + E/D}}\right], \tag{6}$$

where $z = \exp[-\alpha(r - r_0)]$. Here $p$ is the momentum, $\mathrm{sgn}(p)$ is the sign of the momentum, and $\theta$ is the angle variable which runs from $-1/2$ to $1/2$. The classical action $I$ corresponds to the quantum number $\nu$, and tracking it in the phase space gives a clear picture of the evolution of the effective quantum number $\nu$ as the pulse is swept through. Since the energy is a function of $\nu + 1/2$ (equation 2), the smallest action is $-1/2$ and we use $\nu$ instead of action in our plots for clarity. The angle coordinate $\theta$ is a measure of the phase of the classical orbit.

Figure 4 shows the surfaces of section plots for the peak IR intensities of $9 \times 10^{13}$ W cm$^{-2}$ (column 1) and $18 \times 10^{13}$ W cm$^{-2}$ (column 2) before (panels A1 and A2), on (panels B1 and B2), and after (panels C1 and C2) the peaks of the carrier envelopes. These intensities correspond to stars and triangles seen in figure 3 except that in figure 4 we do not chirp the frequencies in order to simplify the classical picture. On top of each surface of section, we plot the phase space positions of the trajectories at corresponding instances during the IR pulse (large filled circles). Before the transition, trajectories reside on the initial stable surface of $\nu = 0$ (panels A1 and A2). These correspond to intensities $5 \times 10^{13}$ W cm$^{-2}$ and $10^{14}$ W cm$^{-2}$ respectively. As the peak intensities of $9 \times 10^{13}$ W cm$^{-2}$ and $18 \times 10^{13}$ W cm$^{-2}$ are reached in B1 and B2, this stable surface is destroyed and the trajectories that were on this surface are mixed into the chaotic sea. Note that for the smaller peak intensity in B1, trajectories stay almost perfectly along the lines that are used to made up the separatrix, even after these surfaces are destroyed by the driving field. More than half of the trajectories mixed into the chaotic sea have swung around the main island of stability. In B2, where the driving field is stronger by a factor of ∼1.4, the trajectories drift and disperse inside the chaotic sea more rapidly compared with A2, resulting in a final wider spread in $\nu$ than in A1, as depicted by the triangles in figure 3. The fact that $\nu$ initially has the lowest possible value at $-1/2$ results in the formation of a stable island centred at $\sim -0.3\pi$ rad (seen more prominently in B1). This island is destroyed in B2 due to the stronger driving field. During the falling edges of the IR pulses with $I = 5 \times 10^{13}$ W cm$^{-2}$ and $I = 10 \times 10^{13}$ W cm$^{-2}$ (C1 and C2 respectively), stable surfaces are formed again and the trajectories are captured onto final stable $\nu$-manifolds. In C1, this means that about half the trajectories end up on the $\nu = 4$ surface and the other half stay on the initial $\nu = 0$ stable surface. A large spread of final $\nu$ is seen in C2 in agreement with the triangles in figure 3.

## 3. Quantum calculations in three dimensions

A detailed account of our fully three-dimensional quantum calculations has been given in [14] for the case of a microwave-driven Rydberg atom. The difference in the molecular case is only in the radial part of the Hamiltonian describing the vibrational potential and in the dipole coupling as a function of $r$. The details of the Morse potential and the proper dipole function used in the interaction Hamiltonian for HF were described in section 2.2 for the one-dimensional treatment of the problem. The interaction Hamiltonian itself now couples $J$ to $J \pm 1$ since it is now $-\mathcal{F}(t)\mu\cos(\theta)$. In this way, the three-dimensional calculations take into account the role of the rotational levels as they are coupled with the vibrational degree of freedom as a result of the interaction with the IR laser pulse.

Figure 5 shows time-dependent probabilities in vibrational states with $\nu = 0$ through $\nu = 4$ (panel (a)), along with the probabilities in the rotational modes $J = 0$ through $J = 4$ (panel (b)). The peak IR laser intensity, chirp range and carrier envelope width are identical to those used in the one-dimensional quantum simulations presented in figure 1. The molecule starts in the initial rovibrational state of $|\nu = 0, J = 1\rangle$ and is driven up to $|\nu = 4, J = 1\rangle$ through the four-photon resonance condition. The time evolution and the final distributions of the vibrational manifolds are very similar

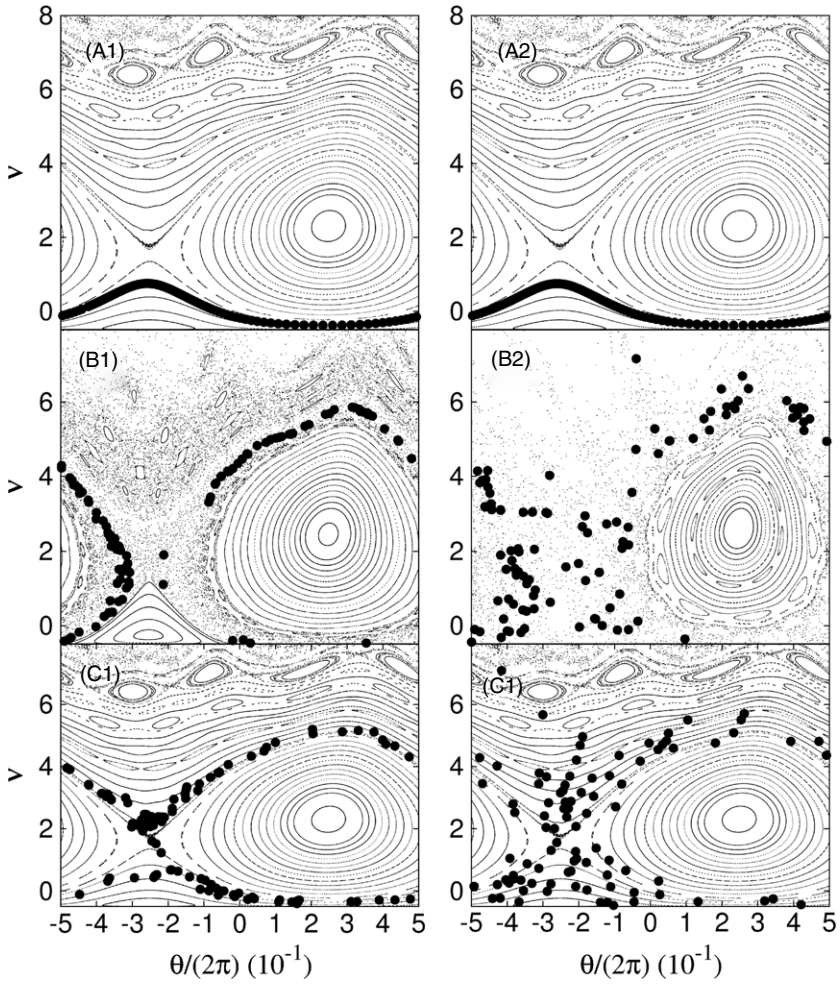


**Figure 4.** Phase space positions of the trajectories from the one-dimensional classical model *without chirp* before (A1 and B1), on (A2 and B2), and after (C1 and C2) the peak of the laser pulse. The right column is for the peak intensity of $9 \times 10^{13}$ W cm$^{-2}$ and the left column is for $18 \times 10^{13}$ W cm$^{-2}$. The large points on top of the surfaces of section are the actual phase space positions of trajectories that started on the $\nu = 0$ stable surface. Note that for the lower peak intensity in B1, the trajectories stay near the positions of the former stable surfaces that made up the separatrix whereas in B2 higher laser intensity dispersed the trajectories inside the phase space.

to those seen in the one-dimensional quantum simulations with the entire population transitioning into the $\nu = 4$ manifold after the IR pulse is turned off. This suggests that the coupling into different rotational pathways is not significantly important for the transition to occur. The probabilities for the rotational quantum numbers evolving in time seen in figure 5(b) suggest that the final rotational mode of the molecule is the one that it started out with i.e. $J = 1$. Only $J = 0$ and $J = 2$, i.e. the adjacent rotational modes get significantly excited during the transition, which transition back into $J = 1$ by the end of the IR pulse. Recall that the transition at this peak intensity stems from tunnelling as we inferred by comparing the one-dimensional quantum and classical simulations.

Population distributions in quantum numbers $\nu$ and $J$ before, on and after the peak of the carrier envelope are seen in figure 6. These snapshots are taken at the same instances during the IR pulse as the one-dimensional wavefunction plots seen in figure 2. At half the peak intensity (leftmost panel), the entire population is in the initial $|\nu = 0, J = 1\rangle$ state, similar to the one-dimensional wavefunction plot in figure 2(a). At the peak of the laser pulse (middle panel), the population has spread out and now spans $J$ up to 3 and $\nu$ up to 5. It is confined mostly in $\nu = 0$, 3 and 4 which can also be seen from figure 5(a). The probabilities display a checkerboard pattern for $J \geqslant 2$; for $J = 2$, $\nu = 0$, 2 and 4, and for $J = 3$, $\nu = 1$, 3 and 5 being populated. This comes from the fact that each absorbed photon can change the angular momentum by one unit and successive $\nu$ are roughly separated by one photon. This is different than the atomic case where the four-photon frequency would correspond to roughly the energy of the state that lies approximately half way between the initial and final states [14, 15]. After field intensity drops back to half the peak value again (rightmost panel), the entire population settles into the final $|\nu = 4, J = 1\rangle$ state.

The conservation of the initial rotational quantum number $J$ after the transitioning can potentially make this method appealing over the ladder climbing scheme in research involving self-imaging of molecules in strong laser fields (see [20] for a detailed account). In this context, self-imaging of a molecule by its own ionized rescattering electron in a strong laser field requires a fair level of alignment of the molecule itself in order for structural information to be recoverable

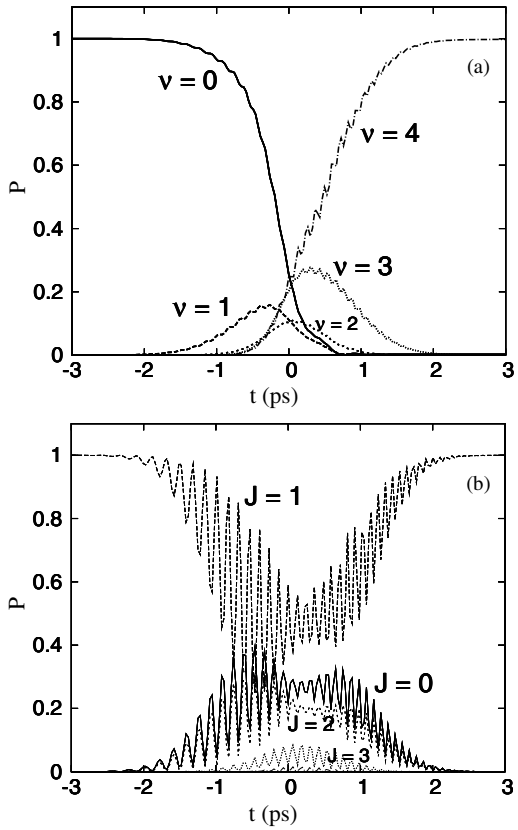


**Figure 5.** (a) Same as figure 1 but from a full three-dimensional simulation with the same set of parameters as those used in the one-dimensional simulations of section 2.2. The HF molecule starts from the $|\nu = 0, J = 1\rangle$ state and is driven up to $|\nu = 4, J = 1\rangle$ through the four-photon resonance condition. (b) Time-dependent evolution of $P$ for $J$ up to 4. ($J = 4$ is the dot-dashed curve at the bottom which we did not label to prevent cluttering.) Although $J = 0$ and $J = 2$ are significantly populated during the pulse, the molecule stays entirely in $J = 1$ after the IR pulse is turned off.

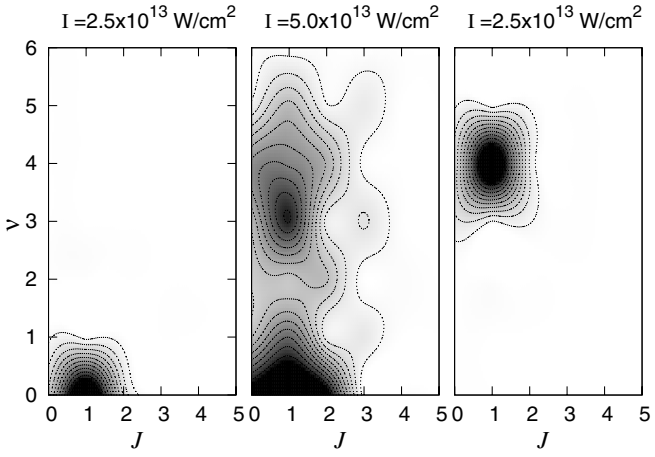


**Figure 6.** ($\nu$,$J$)-distributions for the run presented in figure 5 before (left panel), during (middle panel) and after (right panel) the transition takes place. $P$ is multiplied by 5 in the middle panel for better visibility of smaller structures in the distribution. During the transition, $\nu < 6$ and $J$ remains less than 4.

from the ionization spectrum. Having molecules in excited vibrational states may be desirable for this type of research since the main aim is to watch and steer chemical reactions in real time. Once aligned, vibrational excitation through ladder climbing would destroy the alignment since it would smear the $J$-distribution of the aligned population. This can be circumvented if the multiphoton adiabatic rapid passage scheme is used to vibrationally excite the molecule after it is aligned, preserving the alignment.

## 4. Thermal distribution of rotational levels

The three-dimensional quantum simulations in figure 5 show complete population transfer into the final $|\nu = 4, J = 1\rangle$ state from the ground $|\nu = 0, J = 1\rangle$ state by chirping through a four-photon resonance condition. This would be experimentally challenging to achieve. In the previous section, we have started from a well-defined specific eigenstate $|\nu = 4, J = 1\rangle$ and drove the transition up to another specific final eigenstate. In real-world experiments, the initial state would be smeared over a spectrum of rotational eigenstates as a result of non-zero temperature. In this section, we take into account the effect of this thermal mixing of the initial states on the population transfer. We perform the same calculations as those in section 3 for a series of initial states $|\nu = 0, J\rangle$ for $J$ up to 5 and drive the same four-photon resonance condition using the same chirp range as before. We then average the time-dependent probabilities $P_J$ as

$$P = \frac{\sum_J (2J+1)\, \mathrm{e}^{-\varepsilon_J/k_B T} P_J}{\sum_J (2J+1)\, \mathrm{e}^{-\varepsilon_J/k_B T}}. \tag{7}$$

Here $\varepsilon_J$ is the energy of the eigenstate $|\nu = 0, J\rangle$ relative to the ground state $|\nu = 0, J = 0\rangle$, $k_B$ is the Boltzman constant and $T$ is the temperature. We pick 150 K as the temperature, which gives substantial rotational population up to $J = 4$ for HF. Much lower but still experimentally feasible temperatures as low as ∼14 K leave the entire ensemble in the $J = 0$ ground state for HF. The initial spread in $J$ at 150 K can be seen from the time-dependent probability distribution in figure 7(b) at $t = -3$ ps. It is also plotted as the open squares in figure 8.

Similar to figure 6, figure 7 shows the time evolutions of probabilities for $\nu$ (panel (a)) and $J$ (panel (b)) quantum numbers. Compared with figure 6(a), figure 7(a) shows that ∼10% of the population stays in $\nu = 0$ and the remaining ∼90% transitions into $\nu = 4$ by the end of the pulse. In this case, $\nu = 3$ lingers around a little longer compared to the pure eigenstate case in figure 6(a). Figure 7(b) shows that states with $J = 1$, 3 and 4 stay roughly at the same level of occupation as they started out with, and states with $J = 0$ and $J = 2$ end up with same probabilities after the the pulse is turned off. In other words, roughly 10% of the population in $J = 2$ transitions into states with $J = 0$. The change in the overall $J$-distribution as a result of the transition can be seen in figure 8. The triangles depict the population distribution over the rotational quantum number $J$, and the squares represent the initial thermal distribution inside the $\nu = 0$ manifold.

Another issue of concern in experiments would be the spatial profile of an actual IR laser pulse. Since the laser intensities of interest are in the strong field regime, most

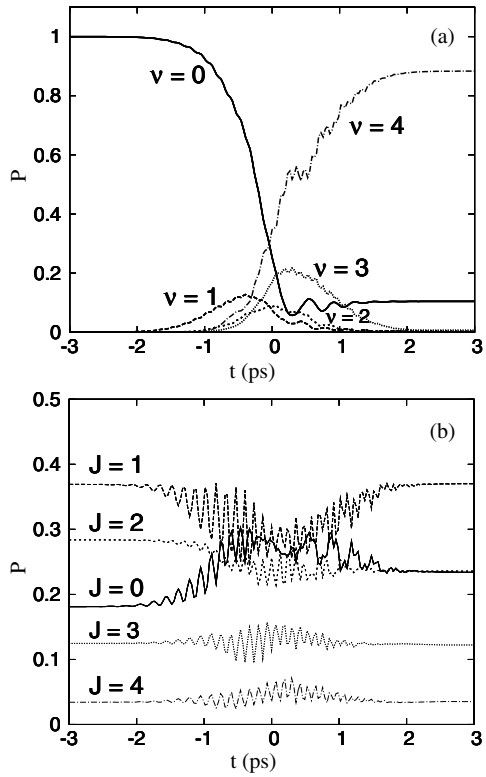


**Figure 7.** Same as figure 5 but starting from a thermal $J$-distribution of states with $\nu = 0$ at 150 K. The initial weights for each $J$-eigenstate of HF at this temperature can be seen at $t = -3$ ps in (b). The total population ended up in the $\nu = 4$ manifold is roughly 12% less than that when the molecule started in an eigenstate in figure 5.

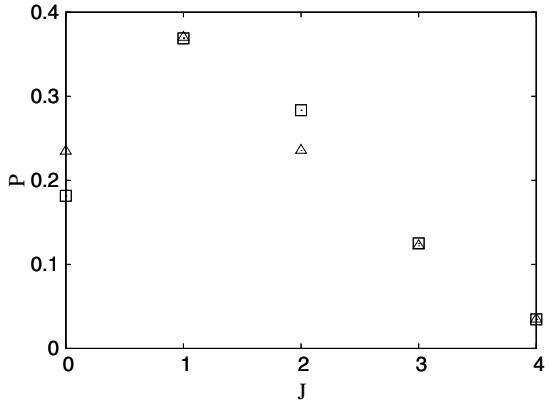


**Figure 8.** Thermal distribution of population over $J$ in the initial $\nu = 0$ manifold (□) and the $J$-distribution after the IR pulse is turned off (△) for 150 K. The peak laser intensity and the pulse duration are the same as those used in figure 5.

likely the laser would need to be focused, resulting in a Gaussian beam profile, for instance. As table 1 indicates, the transition is sensitive to the peak laser intensity. For instance, while $1 \times 10^{13}$ W cm$^{-2}$ results in essentially no transfer at all, twice that would yield complete population transfer into $\nu = 4$. This suggests that in a Gaussian beam, only a small region around the focus would contribute to the transfer, other regions resulting in no transitioning at all. The final averaged picture would qualitatively look like figure 5(a) given that rotational pathways do not play a significant role in how much transfer is attained in each $\nu$-manifold. The amount that transitions into $\nu = 4$ would only weakly depend on how sharply the laser is focused since the transition occurs quite suddenly when a particular laser intensity is reached, as seen from table 1.

## 5. Conclusions

We have presented results of our simulations that show complete population transfer between the ground vibrational state of HF and its $\nu = 4$ excited state by adiabatically chirping through a four-photon resonance condition. This is a demonstration of efficient and robust population transfer in a diatomic molecule which is different from the conventional ladder climbing scheme which has been previously studied. The current method is different than ladder climbing in the sense that it does not involve chirping through a series of intermediate states in a correct order in order to transfer population [4]. The mechanism behind the population transfer is physically identical to that seen in microwave-driven and kicked atoms in the context of population transfer between Rydberg states [13–15].

One-dimensional quantum and classical models show that entire population can be excited up to $\nu = 4$ from the ground state by chirping through a four-photon resonance condition. The chirp required for this is not essential to the physical mechanism, but rather it serves to increase the efficiency of the population transfer. Surprisingly, we also observed that although a peak intensity of $5 \times 10^{13}$ W cm$^{-2}$ results in complete transfer into $\nu = 4$ in the quantum mechanical model, classical model requires at least a peak intensity of $\sim 9 \times 10^{13}$ W cm$^{-2}$ for any transition to occur. This suggests that the complete population transfer in the quantum case with $5 \times 10^{13}$ W cm$^{-2}$ is classically forbidden and happens through tunnelling. For peak laser intensities of $9 \times 10^{13}$ W cm$^{-2}$ and higher, we observe the same separatrix crossing mechanism observed in Rydberg atoms for the multiphoton population transfer. Although $I = 9 \times 10^{13}$ W cm$^{-2}$ results in perfect final-state resolution, intensities up to twice as high result in substantial final state spreads and even dissociation.

By extending our simulations to fully three-dimensional quantum calculations, we introduced the effect of rotational coupling in the excitation process for the four-photon transitioning from the $|\nu = 0; J = 1\rangle$ to $|\nu = 4; J = 1\rangle$ state of HF. Again, we observed complete transfer of population into the final $\nu = 4$ manifold, but this time we also demonstrated that the transferred population entirely retained $J = 1$ character after the IR pulse is turned off. The $J$-states that played a significant role during the transition are only the adjacent $J = 0$ and $J = 2$ states. In order to simulate a more realistic experimental condition, we considered a case where the initial state is not a single rovibrational eigenstate of the field-free HF molecule, but rather a thermal distribution of initial states. We have particularly chosen 150 K as our temperature since this gives a sizable spread in $J$ up to $J = 4$ inside the $\nu = 0$ manifold of HF. For the same set of IR

pulses and chirp ranges used in the one-dimensional and three-dimensional simulations, we have seen that the total fraction of the population transferred into $v = 4$ decreased by only $\sim$10%, and that the final $J$-distribution only differs than that in the beginning of the laser pulse for $J = 0$ and $J = 2$ by roughly 5%.

## Acknowledgments

This work was supported by the Office of Basic Energy Sciences and the Office of Fusion Energy Sciences, US Department of Energy.

## References

[1] Kaluza M, Mukerman J T, Gross P and Rabitz H 1994 *J. Chem. Phys.* **100** 4211
[2] Chelkowski S, Bandrauk A D and Corkum P B 1990 *Phys. Rev. Lett.* **65** 2355
[3] Vrijen R B, Duncan D I and Noordam L D 1997 *Phys. Rev.* A **56** 2205
[4] Maas D J, Vrakking M J J and Noordam L D 1999 *Phys. Rev.* A **60** 1351
[5] Lin J T, Hayashi M and Lin S H 1999 *Phys. Rev.* A **60** 3911
[6] Kallush S and Band Y B 2000 *Phys. Rev.* A **61** 041401
[7] Strasfeld D B, Shim S-H and Zanni M T 2007 *Phys. Rev. Lett.* **99** 038102
[8] de Araujo L E E 2008 *Phys. Rev.* A **77** 033419
[9] Kim J-H, Liu W-K and Yuan J-M 1999 *J. Chem. Phys.* **111** 216
[10] Tesch C M and de Vivie-Riedle R 2002 *Phys. Rev. Lett.* **89** 157901
[11] Dunning F B, Mestayer J J, Reinhold C O, Yoshida S and Burgdörfer J 2009 *J. Phys. B: At. Mol. Opt. Phys.* **42** 022001
[12] Hosaka K, Shimada H, Chiba H, Katsuki H, Teranishi Y, Ohtsuki Y and Ohmori K 1999 *Phys. Rev.* A **60** 3911
[13] Maeda H, Norum D V L and Gallagher T F 2006 *Phys. Rev. Lett.* **96** 073002
[14] Topcu T and Robicheaux F 2009 *J. Phys. B: At. Mol. Opt. Phys.* **42** 044014
[15] Topcu T and Robicheaux F 2010 *J. Phys. B: At. Mol. Opt. Phys.* **43** 115003
[16] Broeckhove J, Feyen B and Leuven P Van 1992 *J. Mol. Struct.* **261** 265
[17] Landau L D and Lifshitz E M 1999 *Quantum Mechanics* (Oxford: Pergamon)
[18] Whaley K B and Light J C 1982 *J. Chem. Phys.* **77** 1818
[19] Connor J N L and Laganà A 1981 *Mol. Phys.* **44** 403
[20] Lin C D, Le A T, Chen Z J and Lucchese R 2010 *J. Phys. B: At. Mol. Opt. Phys.* **43** 122001